Majorana zero-energy modes and spin current evolution in mesoscopic superconducting loop systems with spin-orbit interaction

Guo-Qiao Zha,[1,2,3] Lucian Covaci,[3] F. M. Peeters,[3] and Shi-Ping Zhou[1,2]
[1]*Department of Physics, Shanghai University, Shanghai 200444, China*
[2]*Shanghai Key Laboratory of High Temperature Superconductors, Shanghai University, Shanghai 200444, China*
[3]*Departement Fysica, Universiteit Antwerpen, Groenenborgerlaan 171, B-2020 Antwerpen, Belgium*
(Received 31 July 2015; published 29 September 2015)

The Majorana zero modes and persistent spin current in mesoscopic d-wave-superconducting loops with spin-orbit (SO) interaction are investigated by numerically solving the spin-generalized Bogoliubov–de Gennes equations self-consistently. For some appropriate strength of the SO coupling, Majorana zero-energy states and sharp jumps of the spin-polarized currents can be observed when the highest energy levels cross the Fermi energy in the spectrum, leading to spin currents with opposite chirality flowing near the inner and outer edges of the sample. When the threaded magnetic flux turns on, four flux-dependent patterns of the persistent spin current with step-like features show up, accompanied by Majorana edge modes at flux values where the energy gap closes. Moreover, the Majorana zero mode is highly influenced by the direction of the Zeeman field. A finite in-plane field can lead to the gap opening since the inversion symmetry is broken. Remarkably, multiple Majorana zero-energy states occur in the presence of an out-of-plane field $\mathbf{h}_z$, and the number of steps in the spin current evolution can be effectively tuned by the field strength due to the shift of Majorana zero modes. Finally, when the loop sample contains surface indentation defects, zero-energy modes can always show up in the presence of an appropriate $\mathbf{h}_z$. Interestingly, multiple Majorana states may be present in the system with a corner defect even if $\mathbf{h}_z = 0$.

DOI: 10.1103/PhysRevB.92.094516 PACS number(s): 74.78.Na, 74.20.Rp

I. INTRODUCTION

Superconducting systems with spin-orbit (SO) coupling [1] have attracted a great deal of attention recently [2–19]. With the development of experimental techniques, it is now possible to fabricate nanostructured samples with different shapes. As is well known, structural inversion asymmetry can be created at surfaces, interfaces, or some junction structures. In materials without inversion symmetry, Rashba-type SO interactions lift the spin degeneracy of the electronic bands and generate complex spin textures in the electron Bloch functions. It has been predicted that strong SO interactions in nodal superconductors can give rise to a nontrivial band topology, leading to topologically protected zero-energy edge states [9–15]. Majorana fermions, which are their own antiparticles, can be realized in superconductors even if the symmetry of the gap function is spin-singlet dominant [16–18]. Obviously, the ability of the SO interaction to link the electron charge and spin degrees of freedom provides a fertile ground for novel physical phenomena in mesoscopic superconducting systems.

Motivated by research on unconventional flux periodic evolution in multiply connected superconducting systems [20–29], we recently considered the SO coupling effect in a mesoscopic d-wave-superconducting loop and predicted a possible mechanism that supports fractional flux periodicity [30]. When the SO interaction is involved, the energy spectrum splits and superconducting phase transitions emerge due to the existence of Majorana fermion states. In the present work, we focus on the Majorana zero-energy mode in mesoscopic loop systems and provide a careful insight into its generation and evolution depending on the SO interaction and threaded flux. Moreover, there are still several aspects that remained unaddressed in such mesoscopic loops. For example, how does the Zeeman field, which is an important perturbation for the spin structure of the Cooper pairs, affect the energy spectrum and the Majorana zero mode? Meanwhile, rough surfaces have a strong impact on the local density of states, in particular, for nanosized d-wave loops due to the drastic scattering of nodal quasiparticles [27]. Therefore, these effects should be studied in detail.

In addition, there has been intensive study in the field of spin-dependent transport in nanostructures because potential applications to spin electronic devices and information technologies are expected [31–35]. In order to successfully utilize the spin degree of freedom of electrons, one has to develop various techniques such as the generation of spin-polarized current, manipulation and detection of spin, and spin-relaxation control. It is generally known that the SO interaction, which couples the spin degree of freedom of electrons to their orbital motion [36], gives rise to an useful way to manipulate and control electron spin [37–40] and plays an important role in spintronics. This implies that interesting quantum phenomena related to persistent spin current may be produced in mesoscopic superconducting loops with SO coupling.

In view of the above, we systematically investigate here the novel evolution of Majorana zero modes and persistent spin current in mesoscopic $d_{x^2-y^2}$-wave-superconducting loops by solving the spin-generalized Bogoliubov–de Gennes (BdG) equations [5,8,16,30,41] in a self-consistent manner. Our numerical analysis first tackles the issue of whether the zero-energy Majorana edge mode can exist in mesoscopic nodal loops with only the SO interaction. The dependence of spin-polarized currents on the strength of the SO coupling is also discussed. Then we examine the different evolution patterns of persistent spin currents when the system is threaded by a magnetic flux. Moreover, the novel evolution of the Majorana zero-energy state and corresponding spin current is

shown when the effect of the Zeeman field is included. Finally, the influence of surface indentation defects on the spin current is addressed.

The paper is organized as follows: In Sec. II we present our theoretical formalism. The Majorana zero-energy modes and persistent spin current in mesoscopic loop systems with only SO coupling are discussed in Sec. III. The effects of the Zeeman field and surface defects are given, respectively, in Secs. IV and V. Our results are summarized in Sec. VI.

II. THEORETICAL APPROACH

To investigate the properties of mesoscopic d-wave-superconducting loops whose edges are oriented parallel to the [100] and [010] directions in the presence of the spin-orbit interaction, we start with the pairing Hamiltonian by assuming a nearest-neighbor attraction V for d-wave-superconducting (DSC) pairing:

$$\hat{H} = \hat{H}_0 + \hat{H}_{\rm so}, \tag{1}$$

$$\hat{H}_0 = -\sum_{\langle \mathbf{ij}\rangle,\sigma} t_{\mathbf{ij}}\exp(i\varphi_{\mathbf{ij}})c^\dagger_{\mathbf{i}\sigma}c_{\mathbf{j}\sigma} - \mathbf{h}_z\sum_{\mathbf{i},\sigma,\sigma'}(\sigma_z)_{\sigma\sigma'}c^\dagger_{\mathbf{i}\sigma}c_{\mathbf{i}\sigma'} - \mu\sum_{\mathbf{i},\sigma} c^\dagger_{\mathbf{i}\sigma}c_{\mathbf{i}\sigma} + \sum_{\langle \mathbf{ij}\rangle}(\Delta_{\mathbf{ij}}c^\dagger_{\mathbf{i}\uparrow}c^\dagger_{\mathbf{j}\downarrow} + \Delta^*_{\mathbf{ij}}c_{\mathbf{j}\downarrow}c_{\mathbf{i}\uparrow}), \tag{2}$$

$$\hat{H}_{\rm so} = V_{\rm so}\sum_{\mathbf{i}}\left[\left(c^\dagger_{\mathbf{i}\uparrow}c_{\mathbf{i}+\vec{e}_x\downarrow} - c^\dagger_{\mathbf{i}\downarrow}c_{\mathbf{i}+\vec{e}_x\uparrow}\right) - i\left(c^\dagger_{\mathbf{i}\uparrow}c_{\mathbf{i}+\vec{e}_y\downarrow} + c^\dagger_{\mathbf{i}\downarrow}c_{\mathbf{i}+\vec{e}_y\uparrow}\right) + \text{H.c.}\right], \tag{3}$$

where $t_{\mathbf{ij}} = t$ are the nearest-neighbor hopping integrals and $V_{\rm so}$ is the SO coupling strength. $c_{\mathbf{i}\sigma}$ ($c^\dagger_{\mathbf{i}\sigma}$) are destruction (creation) operators for electrons of spin σ ($\sigma =\uparrow$ or $\downarrow$), and $\vec{e}_x$, $\vec{e}_y$ is the unit vector along the x and y directions, respectively. $(\mathbf{h}_x,\mathbf{h}_y,\mathbf{h}_z)$ describes the Zeeman site energy, and $(\sigma_x,\sigma_y,\sigma_z)$ are the Pauli matrices. $n_{\mathbf{i}\sigma} = c^\dagger_{\mathbf{i}\sigma}c_{\mathbf{i}\sigma}$ is the number operator, and μ is the chemical potential determining the averaged electron density. The Peierl's phase factor is given by $\varphi_{\mathbf{ij}} = \pi/\Phi_0\int_{r_{\rm i}}^{r_{\rm j}}\mathbf{A}(\mathbf{r})d\mathbf{r}$, with the superconducting flux quantum $\Phi_0 = hc/2e$. We choose a vector potential of the form $\mathbf{A}(\mathbf{r}) = (y,-x,0)\Phi/[2\pi(x^2+y^2)]$, only yielding an Aharonov–Bohm flux threading the hole, where $\phi = (2e/hc)\Phi$ measures the flux in units of Φ_0. The DSC order has the following definition: $\Delta_{\mathbf{ij}} = V\langle c_{\mathbf{i}\uparrow}c_{\mathbf{j}\downarrow} - c_{\mathbf{i}\downarrow}c_{\mathbf{j}\uparrow}\rangle/2$. By using the Bogoliubov transformation, $c_{\mathbf{i}\sigma} = \sum_n[u^n_{\mathbf{i}\sigma}\gamma_{n\sigma} - \sigma v^{n*}_{\mathbf{i}\sigma}\gamma^\dagger_{n\bar{\sigma}}]$, the Hamiltonian in Eq. (1) can be diagonalized by solving the resulting BdG equations self-consistently,

$$\sum_{\mathbf{j}}^{N}\begin{pmatrix}\mathcal{H}_{\mathbf{ij}\uparrow} & V_1^{\rm so} & 0 & \Delta_{\mathbf{ij}}\\ V_2^{\rm so} & \mathcal{H}_{\mathbf{ij}\downarrow} & \Delta_{\mathbf{ij}} & 0\\ 0 & \Delta^*_{\mathbf{ij}} & -\mathcal{H}^*_{\mathbf{ij}\uparrow} & V_3^{\rm so}\\ \Delta^*_{\mathbf{ij}} & 0 & V_4^{\rm so} & -\mathcal{H}^*_{\mathbf{ij}\downarrow}\end{pmatrix}\begin{pmatrix}u^n_{\mathbf{j}\uparrow}\\ u^n_{\mathbf{j}\downarrow}\\ v^n_{\mathbf{j}\uparrow}\\ v^n_{\mathbf{j}\downarrow}\end{pmatrix} = E_n\begin{pmatrix}u^n_{\mathbf{i}\uparrow}\\ u^n_{\mathbf{i}\downarrow}\\ v^n_{\mathbf{i}\uparrow}\\ v^n_{\mathbf{i}\downarrow}\end{pmatrix}, \tag{4}$$

where $\mathcal{H}_{\mathbf{ij}\sigma} = -t_{\mathbf{ij}}\exp(i\varphi_{\mathbf{ij}}) - (\mathbf{h}_z\sigma+\mu)\delta_{\mathbf{ij}}$, $V_m^{\rm so} = V_{\rm so}\{[(-1)^{m+1}\delta_{\mathbf{i}+\vec{e}_x,\mathbf{j}} + (-1)^m\delta_{\mathbf{i}-\vec{e}_x,\mathbf{j}}] + \lambda_m[i(\delta_{\mathbf{i}+\vec{e}_y,\mathbf{j}} - \delta_{\mathbf{i}-\vec{e}_y,\mathbf{j}})]\}$ ($\lambda_m = -1$ for $m = 1$, 2 and $\lambda_m = 1$ for $m = 3$, 4), and $\delta_{\mathbf{i},\mathbf{j}}$ represents a delta function. With the open boundary conditions (for which the wave function vanishes on the inner and outer boundaries of the loop) we can get the eigenvalues $\{E_n\}$ with eigenvectors $\{u^n_\uparrow, u^n_\downarrow, v^n_\uparrow, v^n_\downarrow\}$. The order parameter $\Delta_{\mathbf{ij}}$ is calculated self-consistently from

$$\Delta_{\mathbf{ij}} = \sum_n\frac{V}{4}\left(u^n_{\mathbf{i}\uparrow}v^{n*}_{\mathbf{j}\downarrow} + u^n_{\mathbf{j}\downarrow}v^{n*}_{\mathbf{i}\uparrow} + u^n_{\mathbf{i}\downarrow}v^{n*}_{\mathbf{j}\uparrow} + u^n_{\mathbf{j}\uparrow}v^{n*}_{\mathbf{i}\downarrow}\right)\tanh\left(\frac{E_n}{2k_BT}\right). \tag{5}$$

The DSC order parameter is defined at site $\mathbf{i}$ as $\Delta^d_{\mathbf{i}} = (\Delta^d_{\mathbf{i}+\vec{e}_x,\mathbf{i}} + \Delta^d_{\mathbf{i}-\vec{e}_x,\mathbf{i}} - \Delta^d_{\mathbf{i},\mathbf{i}+\vec{e}_y} - \Delta^d_{\mathbf{i},\mathbf{i}-\vec{e}_y})/4$, where $\Delta^d_{\mathbf{i},\mathbf{j}} = \Delta_{\mathbf{ij}}\exp[i\pi/\Phi_0\int_{r_{\rm i}}^{(r_{\rm i}+r_{\rm j})/2}\mathbf{A}(\mathbf{r})d\mathbf{r}]$.

The bond current density $J_{\mathbf{ij}\sigma}$ from lattice site $\mathbf{i}$ to $\mathbf{j}$ is

$$J_{\mathbf{ij}\sigma} = -4\frac{et}{\hbar c}\sum_{n,\sigma}\text{Im}\left(\left\{u^n_{\mathbf{j}\sigma}u^{n*}_{\mathbf{i}\sigma}f(E_n) + v^{n*}_{\mathbf{j}\sigma}v^n_{\mathbf{i}\sigma}[1-f(E_n)]\right\}\exp(i\varphi_{\mathbf{ij}})\right), \tag{6}$$

where $f(E) = (e^{E/k_BT}+1)^{-1}$ is the Fermi–Dirac distribution function. The current $J_{\mathbf{i}\sigma}$ is defined as the average of the neighboring bond currents: $J_{\mathbf{i}\sigma} = [(J_{\mathbf{i}-\vec{e}_x,\mathbf{i},\sigma} - J_{\mathbf{i}+\vec{e}_x,\mathbf{i},\sigma}) + (J_{\mathbf{i},\mathbf{i}-\vec{e}_y,\sigma} - J_{\mathbf{i},\mathbf{i}+\vec{e}_y,\sigma})]/2$. We can determine the local charge and spin current [19,42–44] $J_c(\mathbf{i}) = J_{\mathbf{i}\uparrow} + J_{\mathbf{i}\downarrow}$ and $J_s(\mathbf{i}) = J_{\mathbf{i}\uparrow} - J_{\mathbf{i}\downarrow}$, respectively. Note that the total circulating current J_σ is evaluated through summing $J_{\mathbf{i}\sigma}$ over all lattice sites on the cross section of the middle of the loop's arm.

Throughout this work, the distance is measured in units of the lattice constant a, the energy in units of t, the magnetic flux in units of $\Phi_0 = hc/2e$, and the current density in units of $J_0 = et/\hbar c$. In the numerical calculations, we take $k_B = a = t = 1$ for simplicity and only consider the half filled case, i.e., $\mu = 0$. We focus on the square loop as schematically shown in Fig. 1 with an outer size of $N_x \times N_y$ and a centered hole of size $N_{xx}\times N_{yy}$, which is threaded by a magnetic field Φ in the hole. $w = (N_{x(y)} - N_{xx(yy)})/2$ is the arm width of the sample.

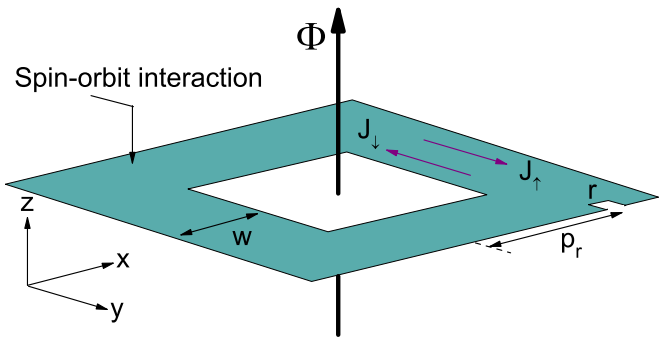

FIG. 1. (Color online) Schematic view of the two-dimensional square loop with spin-orbit interaction, which is threaded by a magnetic flux Φ in the hole. w is the arm width of the sample. r is the size of a small, square indentation at the outer surface of the sample, and p_r is the distance of the defect away from the edge center.

III. MAJORANA EDGE MODES IN MESOSCOPIC LOOPS WITH ONLY SPIN-ORBIT INTERACTION

It is well known that a persistent charge current is induced in a mesoscopic ring with a perpendicular magnetic flux. By analogy, the SO interaction can generate an effective orbital magnetic field, and a persistent spin current should be induced when the SO interaction replaces the perpendicular magnetic flux. In this section, we consider the mesoscopic d-wave-superconducting loop with only the SO interaction and clarify how the zero-energy Majorana edge state emerges in this system in the absence or presence of a threaded magnetic flux. We examine this effect for a perfect square loop with a fixed size $N_x \times N_y = 40 \times 40$ and a fixed arm width $w = 10$ at zero temperature in the following.

A. In the absence of a threaded flux

We start our investigations with a system in the absence of a threaded flux and demonstrate the influence of the SO interaction on the spin current. Figure 2(a) gives the evolution of the spin-polarized currents $J_\uparrow$ and $J_\downarrow$ as a function of SO coupling strength V_{so} when the flux $\Phi = 0$. The d-wave-pairing interaction is taken to be $V = 1.2$. From Fig. 2(a), we can clearly see that, in the presence of SO coupling, the current is spin polarized with opposite orientations for spin-up and spin-down electrons. The persistent charge current is found to be zero because the system exhibits time-reversal symmetry. Therefore, a pure persistent spin current (without an accompanying charge current) can be induced solely by the SO-coupling effect. Figure 2(b) displays the corresponding energy spectrum in the gap region. Notice that we present the order parameter Δ for the average of Δ_i^d over all lattice sites. Normally, the eigenvalues are fourfold degenerate for our superconducting loop. As the SO interaction is included, the degenerate energy levels split while maintaining the twofold Kramers degeneracy. This can be clearly seen from the energy levels closest to E_F in Fig. 2(b). A considerable spectral gap appears for chosen pair interaction $V = 1.2$ when $V_{so} = 0$. Due to the breaking of spin-reversal symmetry for particles and holes in the presence of SO coupling, there is a distinct spin splitting in the energy spectrum with finite V_{so}.

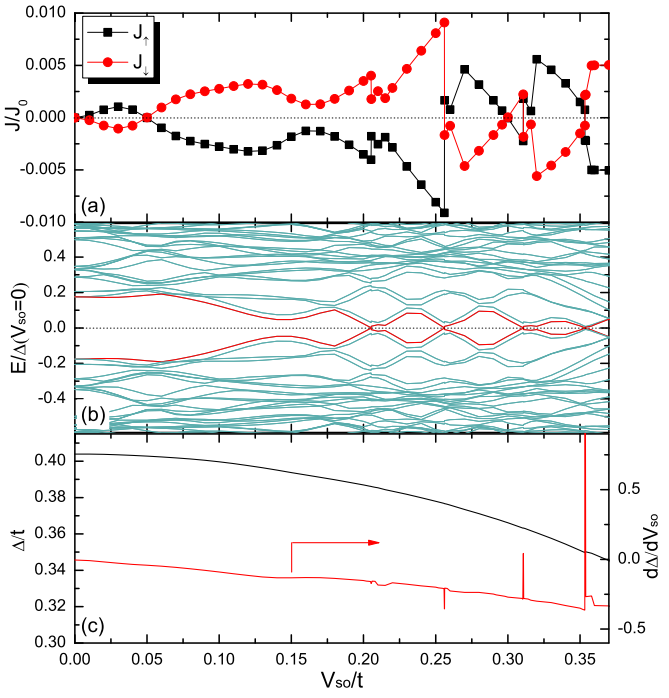

FIG. 2. (Color online) (a) Spin-polarized currents $J_\uparrow$ and $J_\downarrow$, (b) the eigenenergies in the gap region and (c) the order parameter for a square 40×40 loop with an arm width $w = 10$ as a function of SO-coupling strength V_{so} when the threaded magnetic flux $\Phi = 0$. The pair interaction $V = 1.2$, and the temperature $T = 0$. The black dotted line in panel (b) corresponds to the Fermi energy $E_F = 0$.

Interestingly, besides the spin splitting, there appears an oscillating effect of the SO coupling on the superconducting pairing due to the nodal character of the order parameter. The energy gap in Fig. 2(b) is periodically enlarged or reduced while varying V_{so}, as displayed by the red curves. Correspondingly, the spin-polarized currents exhibit oscillatory patterns with V_{so} in Fig. 2(a). The magnitude of $J_{\uparrow(\downarrow)}$ increases initially and then oscillates for stronger V_{so}. At a certain V_{so}, there is a sign change of the current in the curves. We may attribute the reversal of the current direction due to the crossing of levels with opposite spin. With increasing V_{so}, the states further away from the Fermi level $E_F = 0$ provide most of the condensation energy, but the main contribution to the current arises from the occupied levels close to E_F. The direction of persistent spin-polarized currents may be largely determined by the momentum of the highest energy levels. In particular, there generally exists a destructive effect of the SO coupling on the superconducting pairing [see Fig. 2(c)]. The split states are pushed toward the Fermi energy in Fig. 2(b) and the energy gap closes for several appropriate V_{so} values. In Fig. 3, we depict the contour plots of $J_{i\uparrow}$ [Fig. 3(a)] and $J_{i\downarrow}$ [Fig. 3(b)] in the loop when $V_{so} = 0.311$ with a closed gap. Obviously, the spin-up and spin-down currents flow oppositely, and a pure persistent spin current circulates in the loop. The separation of current channels with opposite directions becomes remarkable as the energy gap tends to close and the spin currents mainly appear near the inner and outer edges of the sample, i.e., the zero-energy Majorana edge mode shows up in this system. Notice that, because of the energy-level crossing E_F, superconducting phase transitions appear and the spin-polarized currents show abrupt jumps at the gapless

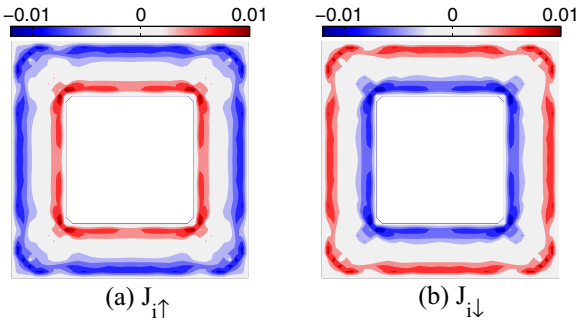

FIG. 3. (Color online) Contour plots of the spin-polarized currents (a) $J_{i\uparrow}$ and (b) $J_{i\downarrow}$ for a square 40×40 loop with $V_{so} = 0.311$ and $w = 10$ at $\Phi = 0$.

points [see also the peaks in the derivative of Δ with respect to V_{so} in Fig. 2(c)].

B. In the presence of a threaded flux

Next, we discuss the modes of Majorana zero-energy states and the corresponding evolution of persistent spin currents at finite threaded magnetic flux. In this case, the equality of the spin-up and spin-down current components of the pure spin current is broken and a net charge current appears. In our previous studies [30], we found that, in mesoscopic nodal superconducting loops with SO coupling, the density of states is finite close to E_F. For an appropriate SO-coupling strength, the energy gap closes at several flux values and Majorana zero modes can be realized at the edges of the square system. Here, we present four representative zero-energy modes to reveal mainly how persistent spin currents evolve as a function of flux. Note that possible phase transitions between condensate states with different winding numbers of the order parameter are neglected. Figure 4 shows the persistent spin current J_s (the solid curves) as well as the spin-polarized currents $J_\uparrow$ (the dashed curves) and $J_\downarrow$ (the dash-dotted curves) for a square 40×40 loop with $w = 10$ as a function of Φ when $V_{so} = 0.2$ [Fig. 4(a)], $V_{so} = 0.24$ [Fig. 4(b)], $V_{so} = 0.27$ [Fig. 4(c)], and $V_{so} = 0.29$ [Fig. 4(d)]. In order to demonstrate clearly the flux evolution of the spin current, the magnitude of J_s is always given by the right-hand scale. At zero flux, the spin current changes its sign for values of V_{so} around 0.25 as shown in Fig. 2(a). With increasing flux, it is found that the spin-polarized currents show, in general, sawtooth patterns. The zigzag-like jumps correspond to the superconducting-ground-state evolution between different energy parabolas [30]. $J_\uparrow$ and $J_\downarrow$ show standard linear behavior and changes synchronously, and the magnitude of $J_s = J_\uparrow - J_\downarrow$ almost takes a constant value for the flux regimes belonging to different energy parabolas. In addition, due to the phase transitions between these flux regimes, J_s is discontinuous and evolves stepwise with flux. Notably, at the flux with closed energy gap in Figs. 4(b) and 4(c), J_s changes its sign due to the relative magnitude for $J_\uparrow$ and $J_\downarrow$ switching in different flux regimes.

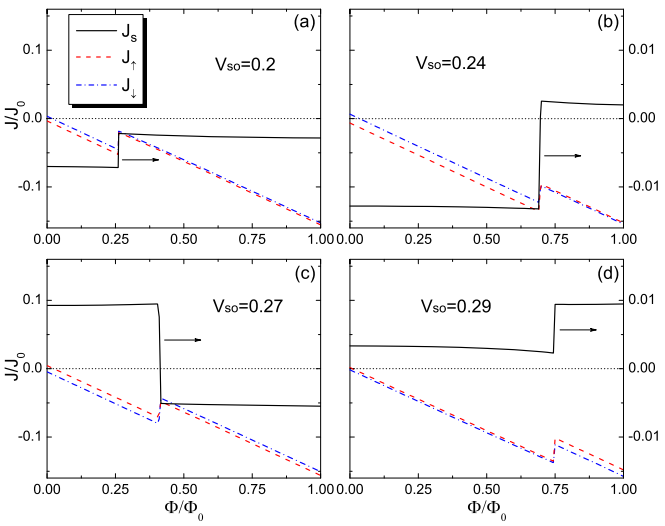

FIG. 4. (Color online) Persistent spin current J_s (right-hand scale) and spin-polarized currents $J_\uparrow$ and $J_\downarrow$ (left-hand scale) for a square 40×40 loop with $w = 10$ as a function of Φ when (a) $V_{so} = 0.2$, (b) $V_{so} = 0.24$, (c) $V_{so} = 0.27$, and (d) $V_{so} = 0.29$. The calculation is performed for $V = 1.2$ and $T = 0$.

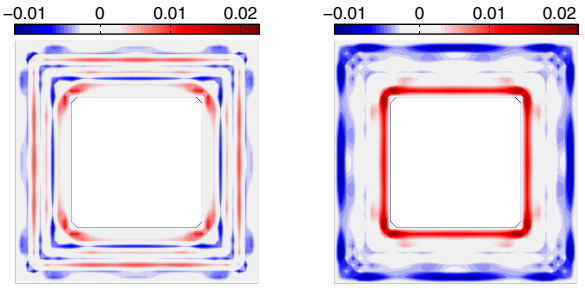

FIG. 5. (Color online) Contour plots of spin current $J_s(\mathbf{i})$ for a square 40×40 loop with (a) $V_{so} = 0.2$ and $w = 10$ at $\Phi = 0$ and (b) at the crossing point $\Phi = 0.262\Phi_0$.

Notice that the emergence of zigzag-like jumps in Fig. 4 may support the existence of Majorana edge states in mesoscopic loop systems in the presence of SO coupling. In this case, the energy gap is closed in the corresponding spectrum at the flux where the current jumps [see also Fig. 8(a) in subsequent Sec. IV]. In order to examine the spin-current distribution related to the Majorana fermion state, Fig. 5 depicts contour plots of the spin current at zero flux [Fig. 5(a)] and at the crossing point $\Phi = 0.262\Phi_0$ with zero energy gap [Fig. 5(b)] for the case of $V_{so} = 0.2$ seen in Fig. 4(a). At zero flux in Fig. 5(a), the pure spin currents with opposite directions are flowing in the current channels of the whole sample. Interestingly, for finite flux and such that Majorana zero-energy modes exist in Fig. 5(b), the persistent spin currents mainly emerge at the edges of the loop with opposite chirality in contrast to the zero-flux case.

IV. EFFECT OF A ZEEMAN FIELD

In a real flux-threaded superconducting loop, the magnetic flux may penetrate into the superconductor itself. From a practical perspective, the external magnetic field can be a Zeeman field, which has a particularly important effect on the spin structure of the Cooper pairs. Moreover, in previous studies on topological superconducting ribbons with SO interations [14–19], the Zeeman field is a necessary condition to realize non-Abelian topological order and Majorana fermions. In this section, we discuss the effect of a Zeeman field on the Majorana edge state and persistent spin current in d-wave mesoscopic loops in the presence of SO coupling. Note that we neglect the orbital effect of the field since it does not change our results qualitatively.

A. With an out-of-plane Zeeman field

For an out-of-plane Zeeman field with $\mathbf{h}_x = \mathbf{h}_y = 0$, we first consider the case of a system without a threaded flux. In order to display clearly the Zeeman field effect, we choose a relative small strength $V_{so} = 0.2$ at zero temperature. Figure 6(a) shows the spin-polarized currents, $J_\uparrow$ and $J_\downarrow$, versus the

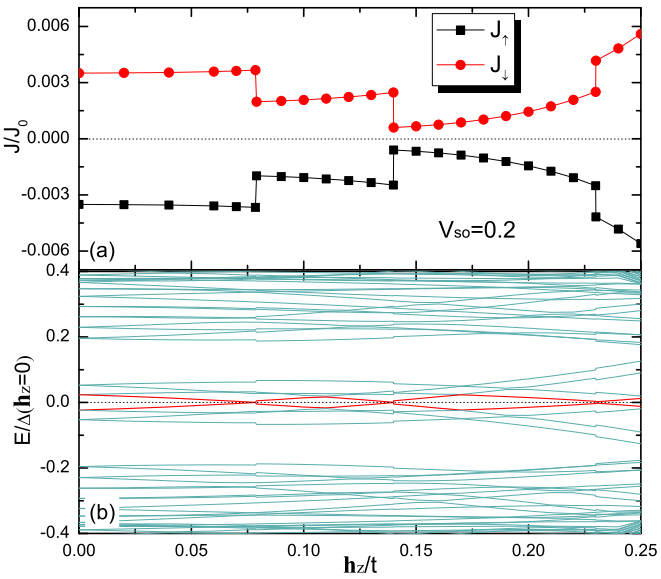

FIG. 6. (Color online) (a) Spin-polarized currents $J_\uparrow$ and $J_\downarrow$ and (b) the eigenenergies in the gap region for a square 40×40 loop with $V_{so} = 0.2$ as a function of out-of-plane Zeeman energy $\mathbf{h}_z$ when the threaded magnetic flux $\Phi = 0$. The pair interaction $V = 1.2$, and the temperature $T = 0$. The black dotted line in panel (b) corresponds to the Fermi energy $E_F = 0$.

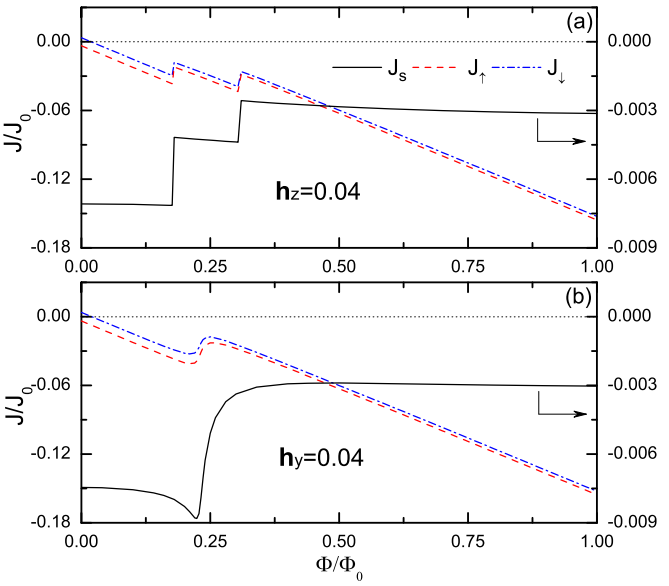

FIG. 7. (Color online) Persistent spin current J_s (right-hand scale) and spin-polarized currents $J_\uparrow$ and $J_\downarrow$ (left-hand scale) for a square 40×40 loop with $w = 10$ and $V_{so} = 0.2$ when (a) $\mathbf{h}_z = 0.04$ and (b) $\mathbf{h}_y = 0.04$. The calculation is performed for $V = 1.2$ and $T = 0$.

strength of the out-of-plane field $\mathbf{h}_z$ for a square 40×40 loop with $w = 10$ when $\Phi = 0$. To understand better the influence of the Zeeman field, the corresponding eigenenergies near the Fermi energy in the gap region are shown in Fig. 6(b). We can see that, once the Zeeman field is introduced, more pronounced spin-split phenomena in the energy spectrum occur. The main contribution to the current evolution arises from the occupied levels closest to E_F (the red curves). Obviously, there exist several zero-energy states in the spectrum, leading to current jumps at the gapless points in Fig. 6(a).

When a finite flux is threaded in the hole, the energy spectrum and the persistent spin current will be modulated further. As a representative example, Fig. 7(a) displays the persistent spin current J_s (the solid curves) and the spin-polarized currents $J_\uparrow$ (the dashed curves) and $J_\downarrow$ (the dash-dotted curves) for a square 40×40 loop with $w = 10$ as a function of Φ when a small Zeeman energy $\mathbf{h}_z = 0.04$. In the absence of a Zeeman field, there appears a zigzag-like jump of $J_{\uparrow(\downarrow)}$ at the crossing flux due to the SO coupling effect [see Fig. 4(a)]. Interestingly, when the effect of a Zeeman field is involved, the flux where the energy gap closes shifts toward a higher value and a new current jump can emerge at small flux [Fig. 7(a)]. Consequently, the spin current jumps stepwise, and the number of steps can increase when an appropriate Zeeman field is included. We also illustrate the energy spectra corresponding to $\mathbf{h}_z = 0$ [Fig. 7(a)] and 0.04 [Fig. 7(b)] as a function of flux in Fig. 8. One can clearly see in Fig. 8(a) that the eigenvalues almost remain twofold degenerate when $\mathbf{h}_z = 0$. However, the energy levels split obviously in Fig. 8(b) with a nonzero field, resulting in the energy gap closing at two flux values which are exactly the same as the ones where the current jumps are found in Fig. 7(a). That is to say, multiple Majorana fermion states may be present in mesoscopic loop systems with SO coupling when the Zeeman field effect is present.

More interestingly, the Majorana zero mode at finite flux can be effectively tuned by $\mathbf{h}_z$ in our mesoscopic loop system. Figure 9 displays the evolution of J_s as a function of Φ for different values of $\mathbf{h}_z$ when $V_{so} = 0.2$. As shown in Fig. 7(a), the energy gap closes at two flux values for small $\mathbf{h}_z$, accompanied by a step oscillatory pattern of the spin current [see Fig. 9(a)]. When $\mathbf{h}_z$ is enlarged, the spin-split effect in the energy spectrum is enhanced and the closest levels are further pushed toward E_F. Thus, we can notice that the flux range between two zero-energy points becomes wider with increasing $\mathbf{h}_z$, i.e., the two crossing points shift in opposite directions. For some critical $\mathbf{h}_z$, only one gapless point at

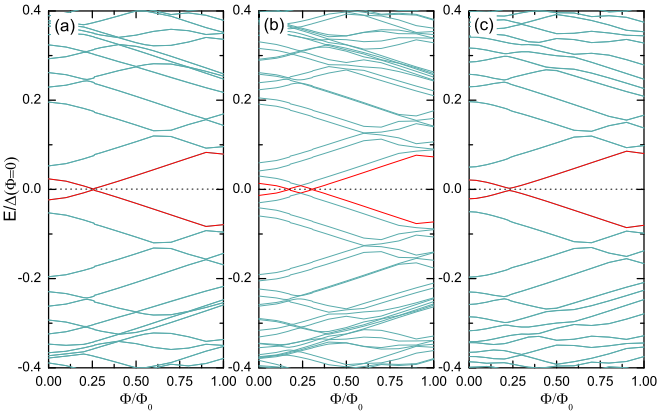

FIG. 8. (Color online) The eigenenergies in the gap region are shown for a square 40×40 loop with $w = 10$ as a function of Φ when (a) $\mathbf{h}_z = 0$, (b) $\mathbf{h}_z = 0.04$, and (c) $\mathbf{h}_y = 0.04$. The red curves correspond to the levels closest to E_F.

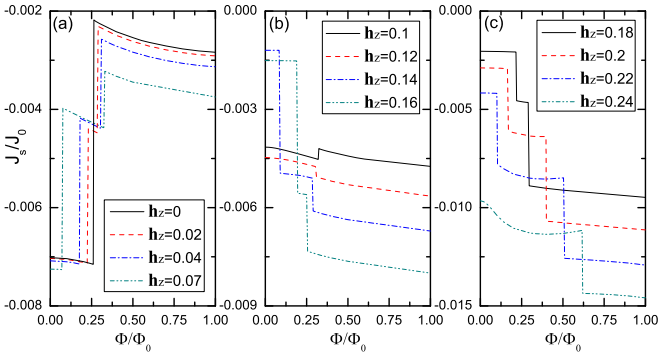

FIG. 9. (Color online) Persistent spin current J_s with different Zeeman energy $\mathbf{h}_z$ as a function of Φ in a square 40×40 loop with $w = 10$. The calculation is performed for $V = 1.2$, $T = 0$, and $V_{so} = 0.2$.

large flux is observed, and the step number of spin current reduces to one [see the black curve in Fig. 9(b)]. Moreover, further increasing $\mathbf{h}_z$ can result in a deviation of the linear feature of the spin-polarized currents near zero flux, and a new gapless point tends to show up again [see the red curve in Fig. 9(b) when $\mathbf{h}_z = 0.12$]. Once the zero-energy state appears, it will keep evolving forward to a higher flux value under the influence of $\mathbf{h}_z$, while another zero-energy point shifts toward zero flux simultaneously. They almost merge together when $\mathbf{h}_z \approx 0.17$ and then shift oppositely once again [see Fig. 9(c)]. As a consequence of the further enlarged Zeeman field, we can observe an evolution process similar to the case in Fig. 9(a).

B. With an in-plane Zeeman field

In this section, we briefly examine Majorana zero modes in the mesoscopic-loop case with an in-plane Zeeman field. For a finite in-plane component $\mathbf{h}_x$ or $\mathbf{h}_y$, it has been found that the gapless edge states are very sensitive to the direction of the applied field due to the breaking of the inversion symmetry [45]. Figure 10 depicts the dependence of $J_\uparrow$ and $J_\downarrow$ on the strength of $\mathbf{h}_y$ [Fig. 10(a)] and the corresponding spectrum in the gap region [Fig. (b)] when $V_{so} = 0.2$ at $\Phi = 0$. In contrast to the out-of-plane case in Fig. 6, the spin-split effect is not obvious and the energy gap always opens in the whole field regime. As a consequence, the step pattern of J_s is smoothed away. Moreover, when a finite flux is applied, the flux evolution of the persistent spin current is also very sensitive to the in-plane field. As seen in Fig. 7(b), while the gapless modes are stable under a Zeeman field in the z direction, they become unstable under a small field in the y direction. By contrast, at a finite $\mathbf{h}_y$ we still find an oscillatory pattern of spin-polarized currents, but the abrupt jumps will be washed out. Correspondingly, the existence of a nonzero $\mathbf{h}_y$ causes a tiny gap in the energy spectrum depicted in Fig. 8(c).

V. THE EFFECT OF SURFACE DEFECTS

Finally, we examine the influence of surface defects on the persistent spin current in mesoscopic d-wave-superconducting loops. Notice that the existence of surface roughness in real experiments is inevitable. Small surface defects strongly affect the flux-induced charge current, which is generally more

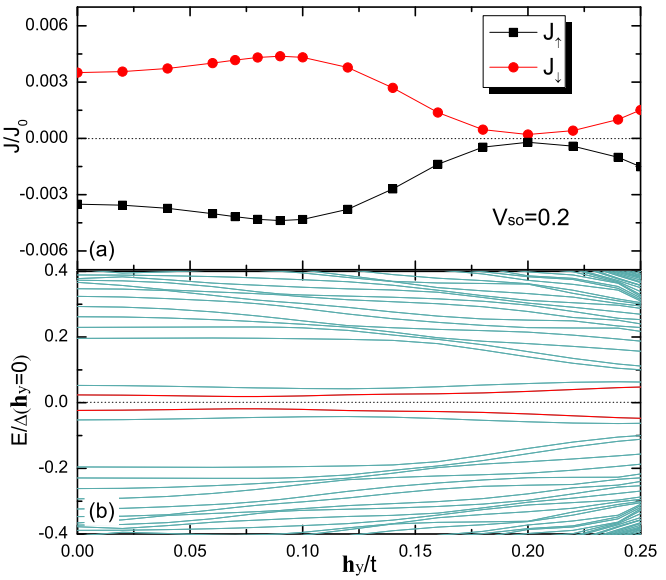

FIG. 10. (Color online) (a) Spin-polarized currents $J_\uparrow$ and $J_\downarrow$ and (b) the eigenenergies in the gap region for a square 40×40 loop with $V_{so} = 0.2$ as a function of in-plane Zeeman field $\mathbf{h}_y$ when the threaded magnetic flux $\Phi = 0$. The pair interaction $V = 1.2$, and the temperature $T = 0$. The black dotted line in panel (b) corresponds to the Fermi energy $E_F = 0$.

sensitive to an indentation than to a bulge [27]. In this study, we restrict ourselves to defects that are small square indentations with size $r \times r = 2 \times 2$ at the outer surface of the sample, as schematically shown in Fig. 1. It is noted that the BdG equations in a two-dimensional lattice have been used to study the effect of surface roughness and the results of the numerical calculations are consistent with experiment [46].

For an indentation defect placed at the center of the edge of the square 40×40 loop (i.e., the defect's distance from the edge center $p_r = 0$), the flux evolution of the spin current J_s is shown in Fig. 11(a) with $V_{so} = 0.2$ and different Zeeman energy $\mathbf{h}_z$. Clearly, the evolution pattern is very sensitive to an indentation. In the absence of a Zeeman field, the zigzag-like patterns of spin-polarized currents shown in Fig. 4(a) for the perfect sample are washed out due to the broken symmetry of the system. Consequently, the step jump of spin currents behaves smoothly, as displayed by the black solid curve in Fig. 11(a). Figure 12(a) gives the corresponding energy spectrum in the gap region. One can see that the closed energy gap in Fig. 8(a) reopens and the current-carrying states of the condensate are continuously changing near the crossing point, which is similar to the case of an asymmetric rectangular loop [30]. Notably, the energy levels with nearly twofold degeneracy in Fig. 8(a) tend to split for the asymmetric system as a result of the quasiparticles reflected on the rough boundary. When the Zeeman field is introduced, the splitting phenomenon in the energy spectrum becomes more remarkable and the highest levels [the red curves in Fig. 12(a)] are pushed toward the Fermi energy. For an appropriate $\mathbf{h}_z$, one can expert to see the gap closing again. With further increasing $\mathbf{h}_z$, two zero-energy states as well as a similar evolution process to the case in Fig. 9 show up, which can be clearly seen by the color curves in Fig. 11(a).

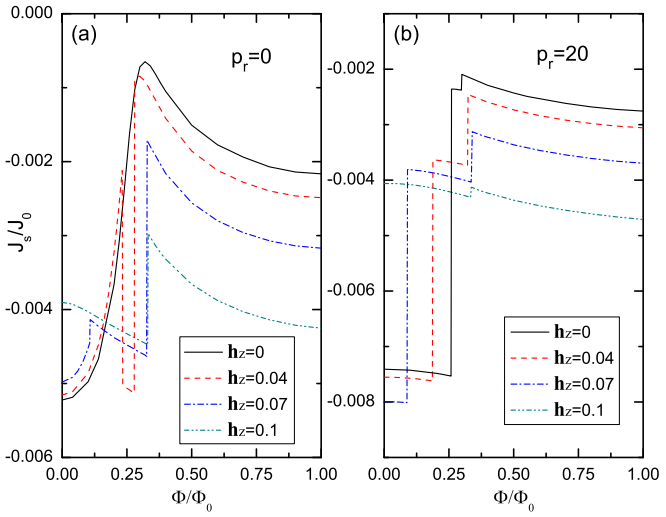

FIG. 11. (Color online) Persistent spin current J_s with different Zeeman energy $\mathbf{h}_z$ as a function of Φ for a square 40×40 loop with a surface $r \times r = 2 \times 2$ indentation (a) at the edge center of the loop with $p_r = 0$ and (b) at the loop's corner with $p_r = 20$. The calculation is performed for $V = 1.2$, $T = 0$, and $V_{so} = 0.2$.

Aside from the indentation defect located exactly in the center of the sample edge, we also checked defects that are displaced to an off-center location from the edge center. As a 2×2 defect is shifted further from the center of the sample edge (not shown here), the corresponding evolution of spin currents with flux is nearly the same as that for the case in Fig. 11(a). Interestingly, for the defect at the loop's corner with $p_r = 20$, the sharply zigzag-like feature of spin-polarized currents appears again even though $\mathbf{h}_z = 0$. Namely, this small

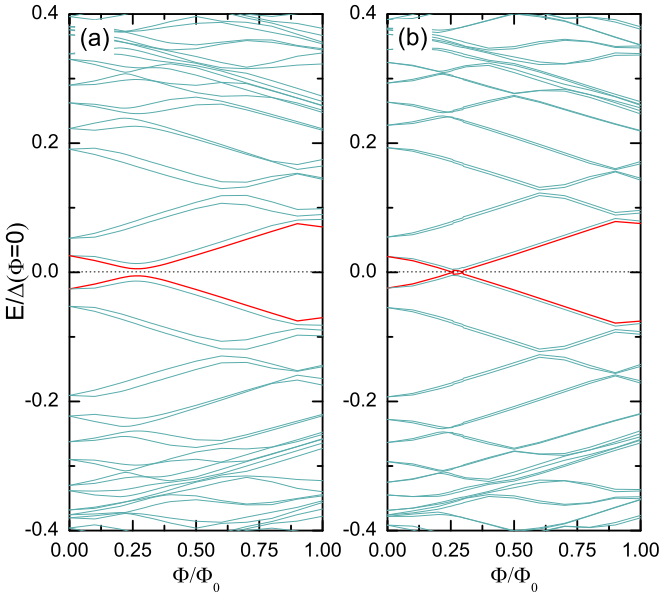

FIG. 12. (Color online) The eigenenergies in the gap region are shown as a function of Φ for a square 40×40 loop with a surface 2×2 indentation (a) at the edge center of the loop with $p_r = 0$ and (b) at the loop's corner with $p_r = 20$ when $\mathbf{h}_z = 0$. The red curves correspond to the levels closest to E_F.

corner defect can play a weakest role in the flux dependence of the persistent spin current. As shown by the black solid curve in Fig. 11(b), the smooth evolution in Fig. 11(a) near $\Phi = 0.26\Phi_0$ is now replaced by a small step oscillation for a defect at the corner due to the occurrence of multiple Majorana zero-energy states, which is similar to the case of a perfect loop with a finite $\mathbf{h}_z$ in Fig. 7(a) [see also the corresponding energy spectrum in Fig. 12(b)]. Furthermore, the flux values where the energy gap closes can also be tuned by the out-of-plane Zeeman field, as depicted in Fig. 11(b).

VI. CONCLUSIONS

In summary, we investigated the Majorana zero mode and persistent spin current in mesoscopic d-wave-superconducting loops in the presence of the SO interaction. We performed numerically self-consistent calculations using the extended BdG equations. The SO coupling effect breaks the spin-reversal symmetry for particles and holes and leads to a distinct spin splitting in the energy spectrum. We found that a pure spin current (without an accompanying charge current) should exist in equilibrium in the mesoscopic loop system due solely to SO coupling. The nonzero spin-polarized currents with opposite directions show an oscillatory behavior with increasing strength of SO coupling, depending on the microscopic details of the energy spectrum. For some appropriate strength of the SO coupling, zero-energy Majorana edge states can be observed when the highest energy levels cross the Fermi energy, leading to sharp jumps of the spin-polarized currents. When a magnetic flux is turned on, a net persistent charge current flows in the system, and the spin-polarized currents show a sawtooth pattern in general. The persistent spin current with step-like features tends to flow near the inner and outer edges of the sample with opposite chirality at the crossing flux due to the existence of Majorana zero modes. Interestingly, four flux-dependent evolution patterns of the spin current can be found for different values of the SO-coupling strength.

In addition, the Zeeman effect on the persistent spin current was studied. It was found that the Majorana zero mode is strongly affected by the direction of the Zeeman field. The zigzag-like flux evolution of the spin-polarized currents can be smoothed away in the presence of a finite in-plane field due to the breaking of the inversion symmetry. However, with increasing an out-of-plane field $\mathbf{h}_z$, the energy gap can close at several flux values and multiple Majorana edge states occur in such systems. Simultaneously, the number of steps in the flux-dependent evolution of the spin current can be effectively tuned by the field strength due to the shift of the Majorana zero mode. Furthermore, the influence of surface defects on the spin current in mesoscopic loops was discussed. In the presence of a small indentation defect at the outer boundary of the sample, the zero-energy states always tend to appear in the presence of an appropriate $\mathbf{h}_z$. Particularly, multiple Majorana zero modes may be present for a corner defect even if $\mathbf{h}_z = 0$.

Our theoretical results clearly demonstrate that the Majorana fermion state and persistent spin current do exist in nodal d-wave loops in the presence of the SO interaction. We expect that our calculations will be useful for future experiments. The spin current may be estimated through the measurable charge current or the induced electric field [47–49],

and its evolution related to the appearance of Majorana zero modes may be detected through the local density of states. Likewise, the modulation of the current evolution might provide an useful way to detect the SO-coupling effects in the superconducting loop system. A promising setup for the experimental detection of Majorana fermions is to exploit an interferometry measurement consisting of a d-wave Rashba superconducting loop, similar to the approach proposed for a superconductor-topological-insulator junction in Refs. [50,51]. Also, a superconducting quantum interference device (SQUID) can be realized by inserting Josephson junctions into a high-T_c superconducting loop. In such a system, the oscillation of the d-wave SQUIDs critical current may have the similar flux-periodic evolution as the circulating supercurrent [52,53]. In addition, possible candidate materials with gap nodes are heavy fermion noncentrosymmetric superconductors, such as $CeRhSi_3$ and $CeIrSi_3$, in which some of time-reversal-invariant k points reside close to the Fermi level [18].

ACKNOWLEDGMENTS

This work was supported by National Natural Science Foundation of China under Grants No. 61371020, No. 61271163, and No. 61571277, by the Visiting Scholar Program of Shanghai Municipal Education Commission, and by the Flemish Science Foundation (FWO-Vl).

[1] E. I. Rashba, Sov. Phys. Solid State **2**, 1109 (1960); Y. A. Bychkov and E. I. Rashba, JETP Lett. **39**, 78 (1984).
[2] V. M. Edelstein, Phys. Rev. Lett. **75**, 2004 (1995).
[3] L. P. Gorkov and E. I. Rashba, Phys. Rev. Lett. **87**, 037004 (2001).
[4] V. V. Kabanov, Phys. Rev. B **69**, 052503 (2004).
[5] B.-L. Gao and S.-J. Xiong, Phys. Rev. B **75**, 104507 (2007).
[6] R. H. Silsbee, J. Phys.: Condens. Matter **16**, R179 (2004).
[7] S. P. Zhou, Y. M. Shi, B. H. Zhu, and G. Q. Zha, Phys. Rev. B **73**, 174503 (2006).
[8] H. Meng, H. W. Zhao, L. F. Zhang, L. M. Shi, G. Q. Zha, and S. P. Zhou, Europhys. Lett. **88**, 17005 (2009).
[9] Y. Tanaka, Y. Mizuno, T. Yokoyama, K. Yada, and M. Sato, Phys. Rev. Lett. **105**, 097002 (2010).
[10] K. Yada, M. Sato, Y. Tanaka, and T. Yokoyama, Phys. Rev. B **83**, 064505 (2011).
[11] A. P. Schnyder and S. Ryu, Phys. Rev. B **84**, 060504(R) (2011).
[12] P. M. R. Brydon, A. P. Schnyder, and C. Timm, Phys. Rev. B **84**, 020501(R) (2011).
[13] A. P. Schnyder, P. M. R. Brydon, and C. Timm, Phys. Rev. B **85**, 024522 (2012).
[14] Y. Tanaka, M. Sato, and N. Nagaosa, J. Phys. Soc. Jpn. **81**, 011013 (2012).
[15] C. L. M. Wong, J. Liu, K. T. Law, and P. A. Lee, Phys. Rev. B **88**, 060504(R) (2013).
[16] M. Sato, Y. Takahashi, and S. Fujimoto, Phys. Rev. Lett. **103**, 020401 (2009); Phys. Rev. B **82**, 134521 (2010).
[17] J. D. Sau, R. M. Lutchyn, S. Tewari, and S. Das Sarma, Phys. Rev. Lett. **104**, 040502 (2010).
[18] M. Sato and S. Fujimoto, Phys. Rev. Lett. **105**, 217001 (2010).
[19] Y. Imai, K. Wakabayashi, and M. Sigrist, Phys. Rev. B **85**, 174532 (2012); **88**, 144503 (2013).
[20] F. Loder, A. P. Kampf, T. Kopp, J. Mannhart, C. W. Schneider, and Y. S. Barash, Nat. Phys. **4**, 112 (2008).
[21] T.-C. Wei and P. M. Goldbart, Phys. Rev. B **77**, 224512 (2008).
[22] V. Vakaryuk, Phys. Rev. Lett. **101**, 167002 (2008).
[23] Y. S. Barash, Phys. Rev. Lett. **100**, 177003 (2008).
[24] V. Juričić, I. F. Herbut, and Z. Tešanović, Phys. Rev. Lett. **100**, 187006 (2008).
[25] F. Loder, A. P. Kampf, and T. Kopp, Phys. Rev. B **78**, 174526 (2008).
[26] F. Loder, A. P. Kampf, T. Kopp, and J. Mannhart, New J. Phys. **11**, 075005 (2009).
[27] G.-Q. Zha, M. V. Milosevic, S.-P. Zhou, and F. M. Peeters, Phys. Rev. B **80**, 144501 (2009); **84**, 132501 (2011).
[28] J.-X. Zhu and H. T. Quan, Phys. Rev. B **81**, 054521 (2010).
[29] F. Loder, A. P. Kampf, and T. Kopp, Phys. Rev. Lett. **111**, 047003 (2013).
[30] G.-Q. Zha, L. Covaci, F. M. Peeters, and S.-P. Zhou, Phys. Rev. B **90**, 014522 (2014).
[31] G. A. Prinz, Science **282**, 1660 (1998).
[32] S. A. Wolf, D. D. Awschalom, R. A. Buhrman, J. M. Daughton, S. von Molnar, M. L. Roukes, A. Y. Chtchelkanova, and D. M. Treger, Science **294**, 1488 (2001).
[33] I. Zutic, J. Fabian, and S. Das Sarma, Rev. Mod. Phys. **76**, 323 (2004).
[34] D. D. Awschalom and M. E. Flatte, Nat. Phys. **3**, 153 (2007).
[35] N. Nagaosa, J. Sinova, S. Onoda, A. H. MacDonald, and N. P. Ong, Rev. Mod. Phys. **82**, 1539 (2010).
[36] R. Winkler, *Spin-Orbit Coupling Effects in Two-Dimensional Electron and Hole Systems* (Springer, Berlin, 2003).
[37] D. Grundler, Phys. Rev. Lett. **84**, 6074 (2000).
[38] J. Nitta, T. Akazaki, H. Takayanagi, and T. Enoki, Phys. Rev. Lett. **78**, 1335 (1997); T. Koga, J. Nitta, T. Akazaki, and H. Takayanagi, *ibid.* **89**, 046801 (2002).
[39] J. B. Miller, D. M. Zumbuhl, C. M. Marcus, Y. B. Lyanda-Geller, D. Goldhaber-Gordon, K. Campman, and A. C. Gossard, Phys. Rev. Lett. **90**, 076807 (2003).
[40] V. P. Mineev and K. V. Samokhin, Phys. Rev. B **72**, 212504 (2005).
[41] P. G. de Gennes, *Superconductivity of Metal and Alloys* (Addison-Wesley, New York, 1994).
[42] K. Kuboki and H. Takahashi, Phys. Rev. B **70**, 214524 (2004).
[43] M. Cuoco, A. Romano, C. Noce, and P. Gentile, Phys. Rev. B **78**, 054503 (2008); A. Romano, P. Gentile, C. Noce, I. Vekhter, and M. Cuoco, Phys. Rev. Lett. **110**, 267002 (2013).
[44] G.-Q. Zha, L. Covaci, F. M. Peeters, and S.-P. Zhou, Phys. Rev. B **91**, 214504 (2015).
[45] M. Sato and S. Fujimoto, Phys. Rev. B **79**, 094504 (2009).
[46] Y. Tanuma, Y. Tanaka, M. Yamashiro, and S. Kashiwaya, Phys. Rev. B **57**, 7997 (1998).
[47] F. Meier and D. Loss, Phys. Rev. Lett. **90**, 167204 (2003).

[48] F. Schutz, M. Kollar, and P. Kopietz, Phys. Rev. Lett. **91**, 017205 (2003); Phys. Rev. B **69**, 035313 (2004).
[49] Q.-F. Sun, H. Guo, and J. Wang, Phys. Rev. B **69**, 054409 (2004).
[50] T. Lindstrom, S. A. Charlebois, A. Ya. Tzalenchuk, Z. Ivanov, M. H. S. Amin, and A. M. Zagoskin, Phys. Rev. Lett. **90**, 117002 (2003).
[51] C. W. Schneider, G. Hammerl, G. Logvenov, T. Kopp, J. R. Kirtley, P. J. Hirschfeld, and J. Mannhart, Europhys. Lett. **68**, 86 (2004).
[52] A. R. Akhmerov, J. Nilsson, and C. W. J. Beenakker, Phys. Rev. Lett. **102**, 216404 (2009).
[53] L. Fu and C. L. Kane, Phys. Rev. Lett. **102**, 216403 (2009).